Journal of Computers Vol. 34 No. 6, December 2023, pp. 185-202
doi: 10.53106/199115992023123406015

Slicing-guided Skeleton Extraction Method for 3D Point Clouds of Human Body

Yan-Ni Zhao[1*], Le Xu[2]

[1] College of Artificial Intelligence, Shaanxi Vocational & Technical College, Xi'an 710100, China
feifei6513@163.com

[2] Thoughtworks Software Technologies (Xi'an) Ltd. Xi'an, 710077, China
xulegll@163.com

Received 15 March 2022; Revised 20 April 2022; Accepted 29 April 2022

Abstract. In the paper, a slicing-guided method is introduced to extract the curve skeleton from the point cloud body model. Firstly, the dominant eigenvector of body model as slicing direction is chosen adaptively, and the input body model is sliced accordingly. each slice is projected and classified into different regions, and the centroid of each region can be considered as initial skeleton point. Then, those skeleton points are removed outside models, and initial skeleton lines are generated by connecting points based on different region of body model. Finally, the two-step post-processing approach is proposed to improve the initial skeleton results for accurate topological analysis. With the branch point merging strategy, the initial skeleton of the model is optimized. Furthermore, the skeleton lines by interpolation optimization are refined and smoothed. Compared with similar skeleton extraction algorithms, the method proposed in the paper has relatively strong robustness and effectiveness, and can be applied to human body model in point cloud data.

Keywords: slicing, point cloud, skeleton extraction, skeleton refinement

1 Introduction

Skeleton is a compact mono-dimensional representation able to provide essential topology for both shape recognition and shape manipulation. Skeleton extraction has been widely used in various applications, such as model segmentation [1-3], animation [4-8], shape retrieval [9-11] and shape modeling [12-13]. Many skeleton extraction methods have been proposed, including high dimensional medial representation [14] and 1D curve representation [15]. To extract satisfactory skeletons from point clouds, however, those methods have been left to be improved, among which robustness and accuracy are two key issues need to be addressed.

A good curve skeleton should possess certain properties, including that homotopic to the input shape, well-centered and reliable in that every boundary point is visible from at least one curve-skeleton location [16]. Most existing skeleton extraction methods require a discrete representation of volume or the surface of the input model. However, many scanning models in computer graphic applications can be used as point clouds, it may cause errors in both geometry and connectivity when converting them to surface representations or discrete representations. In this paper, we focus on 1D skeleton extraction from 3D human body in point clouds.

In the paper, a slicing guided skeleton extracting method is introduced which integrates the advantages of horizontal slicing and region decomposition. The algorithm in the paper can be applied to raw scanned data, and only requires minimal user interaction to extract topologically clean and accurate curve skeletons, that is to say, only the appropriate parameters are set, the satisfactory skeletons can be obtained. The main contributions and advantages of our method include:

1) Curve skeleton extraction from 3D body model represented by point sets without converting into polygonal mesh.

2) A horizontal slicing method is proposed to accurately represent the skeletal candidates.

3) A two-step skeleton process yields an optimized skeleton, which is robust and is not sensitive to noise.

The remainder of this paper is organized as follows: Section II analyzes the representative work for skeleton extraction. Section III and Section IV explain the proposed method and the optimization framework in detail. Section V describes the experimental setup, shows some results, and compares the proposed method with the state of art techniques proposed in the literature. Finally, the last section concludes the paper.

* Corresponding Author

2 Related Work

Many algorithms have been proposed for skeleton extraction. Let's review some representative methods in the following, and refer the reader to the comprehensive survey by Cornea, Min and Jalba's works [14-15]. There have been various approaches to extract the one-dimensional skeleton of a given model. Skeleton extraction based on curvature and geodesic distances [17-19], dihedral angles [20], slippage [21], convex decomposition [22], and shape diameter function [23].

The approaches can be classified into Thinning-based method, Contraction-based method, L1-medial method, ROSA-based method, Distance Transform-based method.

Thinning-based method. Thinning-based method constructs the 1D skeleton by repeatedly removing the boundary of the model. Based on topological refinement, a simple and meaningful skeleton set is generated by alternately executing two morphological operations: iterative refinement and skeleton pruning. The thinning process is the iterative deletion of point until a certain condition is satisfied; the pruning process includes morphological corrosion and expansion operation [14].

Ma and Wan [24] proposed a new thinning algorithm for extracting medial surface on 3d binary images. Ma [25] presented a connectivity preserving fully parallel 3D thinning algorithm. Che [26] introduced a dynamic skeleton algorithm for binary image by combining with thinning method and Snake model technique. Lohou [27] put forward two 3D symmetrical thinning algorithms based on the parallel deletion of P-simple points. Wang [28] presented a Valence Driven Spatial Median (VDSM) algorithm to generate unit-width curve skeleton from non-unit-width skeleton. The thinning-based skeleton extraction method can simplify the original model well, and obtain a good skeleton structure with smooth edge and consistent topology of the original model. However, it requires manual input and constant adjustment of pruning parameters in order to calculate ideal skeleton.

Contraction-based method. Each step of the iterative contraction process is a Laplacian smoothing operation, which is constrained by all the vertices with different weights. Previous methods modify or approximate the mesh geometry by solving the Laplacian system, in which all or one subset of vertices are used as boundary constraint.

In reference [29], the original input mesh which approximated as a least squares mesh is the solution of the uniformly weighted discrete Laplace equation, and this equation used carefully selected subsets of vertices as boundary constraints (called anchors). Recently, Au [30] presented a simple and robust skeleton extraction method based on mesh contraction. Nealen [31] proposed a mesh optimization technique, which spreads the concept of geometric smoothing and parameterized smoothing for constrained Laplacian system. Cao [32] developed a contraction operation that is designed to work on generalized discrete geometry data, particularly point clouds, through local Delaunay triangulation and topological thinning. Tagliasacchi [33] proposed a Mean Curvature Flow based method to extract skeleton shrink. Contraction-based method is based on iterative implicit smoothing operation, able to handle noise, so that it is not sensitive to noise; however, the curve skeleton extraction framework is only applicable to closed model with connectivity, which is due to the geometric contraction that need to define a good Laplacian operator for each vertex.

L1-medial method. L1-medial is a simple and powerful statistical tool that extends variable from univariate to multivariate. It represents a unique global center of a given set of points, with the prominent property that it is robust to outliers and noise.

Tagliasacchi [34] relied on a cylindrical shape prior and sufficiently accurate point normal to compensate for missing data. For raw inputs, noise and outliers need to be pre-filtered by using a scheme such as locally optimal projection (LOP) [35]. In contrast, Huang [36] computed a medial curve skeleton by directly working on a noisy, outlier-ridden, and possibly incomplete raw scan without requiring reliable normal estimation or an assumption of cylindrical shape parts. Without building any point connectivity or estimating point normal, the point samples are directly projected onto their local centers as L1-medians with growing neighborhood, and pushed the projected samples through conditional regularization to obtain a uniform distribution of samples along skeleton branches. Livesu [37] proposed a novel approach to skeleton extraction that takes advantage of the principles of human perception and stereoscopic vision to reconstruct a 3D curve- skeleton of the visual hull of the shape starting from the 2D medial axes of the projections of the object into the image plane. Zimovnov [38] presented an efficient algorithm for 3D distance transform computation for the inner voxels of visual hull. Using 3D distance transform, continuous medial axes of visual hull silhouettes are projected backward form a first approximation for a curve-skeleton. L1-medial based method may miss certain fine-scale structure, and produce erroneous output if the amount of noise or missing data is too large.

Distance Transform-based method. The method defines distance transformation for each interior point of 3D object and detects field ridges in order to obtain a group of candidate voxels [39-40], an approximate medial surface produced when connecting these candidate voxels, however, this process is as unstable as other medial-axis-based methods [41-42].

Other field methods use repulsive forces [43] or radial basis functions [44] to replace distance transform. These methods determine the potential of the interior point by considering a larger set of boundary samples, so they are less sensitive to noise. Then, connecting local extremes form a curve-skeleton by the force following algorithm. These methods are computationally intensive because of using larger boundary regions, and also cause numerical instability due to the calculation of the first or second-order derivatives.

Table 1. The advantages and disadvantages in skeleton extraction algorithms

Method	Advantages	Disadvantages
Thinning-based method	Simplify the original model, obtain a skeleton with good topology	Artificial input trimming parameters and constantly adjust them.
Contraction-based method	Make sure the final curve skeleton and the original object are harmonious, and also deal with noise very well	Request more model points
L1-medial method	Operation directly on raw scan data	Incorrect results when models with noise or missing data.
ROSA-based method	Suitable for missing models	Complexity algorithm
Distance Transform-based method	Low complexity and high efficiency and calculation results are accurate	High complexity and low efficiency
Our method	Extract the skeleton directly without converting the mesh model, high computational efficiency and better effect	The adaptability of the multi-human staggered model needs further studying

The advantages and disadvantages of skeleton extraction algorithms is illustrated in Table 1. Based on the previous research, inspired by the centralization of skeleton and considering the characteristics of body model, an efficient slicing-guided method is proposed with weaker human interaction constrains.

3 System Overview

The paper attempt to approximate skeleton points from their corresponding centers called skeletal candidates for a curve skeleton. The input of our method is unorganized set of human body points . The output is a 1D curve skeleton $X = \{x_i\}$ $P = p_j \subset R^3$, it represents a one-dimensional local center of the shape underlying by input value P . The system overview of the proposed method is shown in Fig. 1. The main steps of the algorithm are as follows.

1) Horizontal slicing: The input human body model is firstly analyzed in order to separate the points into horizontal slices.

2) Initial skeleton extraction: With the horizontal slices, a skeleton is produced for the input model using slice projecting and classification.

Then those skeleton points outside model are removed, and initial skeleton lines are generated by connecting points based on different region of body model, which provides an initial skeleton used in the following skeleton optimization.

3) Skeleton refinement: By incorporating the initial skeleton into interpolation method, an interpolation guided method is developed to extract the complete and optimized curve skeleton from the point cloud.

The method proposed in the paper exhibits the advantages of the slicing guided skeleton extraction method. The skeleton extraction system in the paper is robust and effective, and can be applied to human body model in point cloud data.

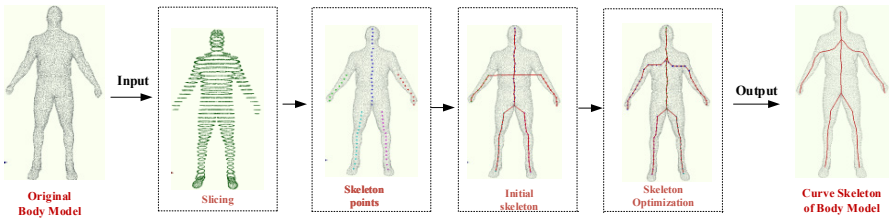

Fig. 1. Overview of our method

4 Technical Details

4.1 Initial Model Normalization

The 3D model should be normalized in older to obtain accurate skeleton. The classical PCA is adopted to determine the main trend of model. The local covariance matrix of 3D point set $P = \{p_1, p_2, \ldots, p_n\}$ is formatted as

$$M = \frac{1}{n}\sum_{i=1}^{n}(p_i - p_m)(p_i - p_m)^T. \quad (1)$$

where $p_m = \sum_{i=1}^{k} p_i$. The local covariance matrix M is always symmetric positive semi-definite, which has three non-negative and ordered eigenvalues, i.e., $\lambda_1 > \lambda_2 > \lambda_3$. The main trend could be considered as the eigenvector v_1 corresponding to λ_1. Fig. 2 displays the main trend (line in green color) of three different body models.

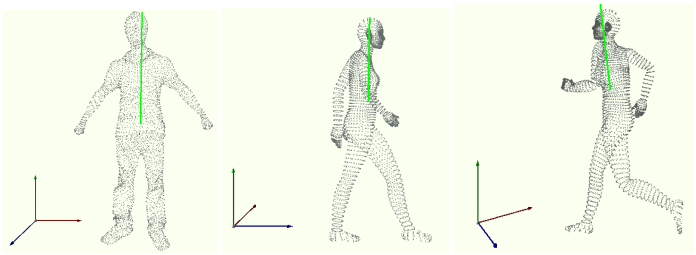

Fig. 2. Main trend of 3D point cloud models

Generally, the human body model is located at any position in the 3D coordinate system. In order to obtain more robust skeleton, The model needs to be rotated according to the Oriented Bounding Box (OBB) of the model. The angle α between OBB and YOZ is calculated, and the angle β between OBB and XOY is also calculated. Taking α and β as the rotation angle, the model is rotated around Z axis and X axis, and finally the model is perpendicular to XOZ plane. For point $p(x, y, z)$, it is rotated around X, Y and Z axis. The model after rotation is shown in Fig. 3.

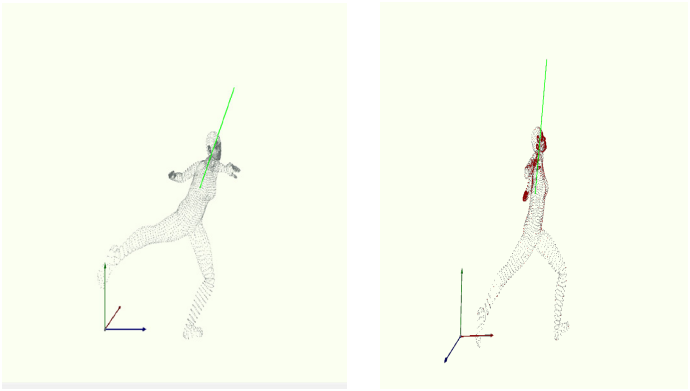

Fig. 3. Rotation of three-dimensional model

4.2 Horizontal Slicing

After normalization, it is assumed that the 3D point model is vertical and perpendicular to XOZ plane. In this step, the 3D model in point cloud is partitioned into h number of horizontal slices along the vertical direction such as the slices shown in Fig. 4.

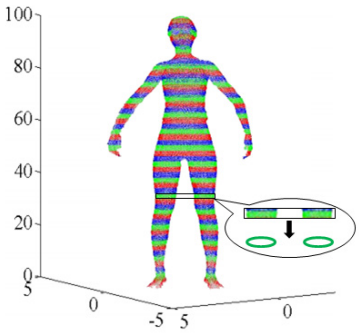

Fig. 4. Horizontal slicing of point cloud model

Horizontal Slicing. All the points in each slice are perpendicularly projected across the middle plane, multiple areas are generated in Fig. 5(a). Each slice of the projection is divided into multiple regions to obtain the central point of each region. The projection regions are decomposed into independent regions ("1" area (red), "2" area (black) and "3" area (blue)) by grid growth algorithm. Then the center point set $O = \{o_1, o_2, \ldots, o_i\}$ for those slices is generated by L_1 median method.

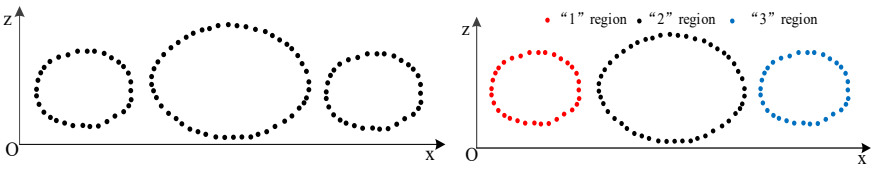

(a) Projection region (b) Region decomposition

Fig. 5. The multiple regions division of slicing projection

Definition 1. Reference layer. Bottom-up horizontal slices that have the largest number of regions are considered as a reference layer L.

The center point $O = \{o_1, o_2, \ldots, o_i\}$ located on different part of human body model should be distinguished. Given point $p(x_1, y_1, z_1)$ in reference layer L and point $q(x_2, y_2, z_2)$, of which the distance is within the slice thickness h, then p and q belong to one part.

$$h = (y_{\max} - y_{\min}) / m\_layerTotal. \tag{2}$$

where $y_{\max}$ and $y_{\min}$ are respectively the maximum and minimum of y coordinate, m_layerTotal is the total slices of 3D model. After this iteration, the region centers that are labeled in different colors shown in Fig. 6.

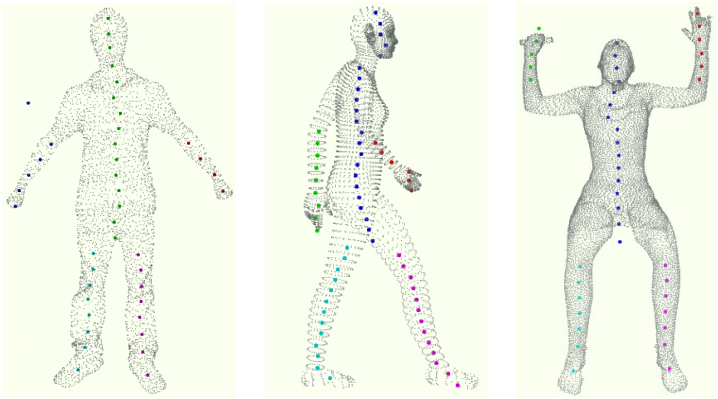

Fig. 6. Center points labeling

Skeleton Candidate Points. Due to the special structure of the human body, the area of the body part is always larger than that of limb. Based on this, we can distinguish the body part in order to achieve the topology structure.

Area of projection region. A strip with width μand perpendicular to X axis, is used to divide the entire projection area, as shown in Fig. 7. The area S of the projection region can be calculated by $S = \sum_{i=1}^{K} S_i = \sum_{i=1}^{K} \left[\mu \times \left(\frac{1}{n_1} \sum_{j=1}^{n_1} z_i - \frac{1}{n_2} \sum_{t=1}^{n_2} z_t \right) \right]$, where μ is the width of the strip, $K = \left\lceil \left(x_{\max} - x_{\min} \right) / \mu \right\rceil$, n_1 is the point number in upper half of rectangle, n_2 is the point number in lower half of the rectangle.

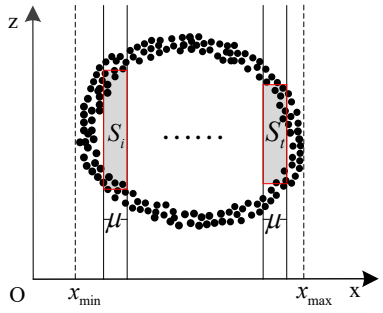

Fig. 7. Calculate the area of projection

Body part determination. The area of different regions in the reference layer L is computed as s_1, s_2, …, s_i. Choose the one that has the largest area and mark it as "M", i.e., the body part, the rest of the regions is marked "N" which is limbs. The point iteration method is used to solve the point classification and then all region center points of body are marked as "M" and region center of limbs are marked as "N".

Skeleton point generation. The center point of the classified model could be converted to skeleton points set as $SK = \{s_1, s_2, \ldots, s_i\}$, which contains not only the coordinate of skeleton point, but the degree, the position, label number and the body part or not. Most of the skeleton points are located in the center of object model, however, there are also a small amount of skeleton points that are located outside the model in Fig. 8. We must remove the model outside the skeleton points to obtain more accurate skeleton candidate points.

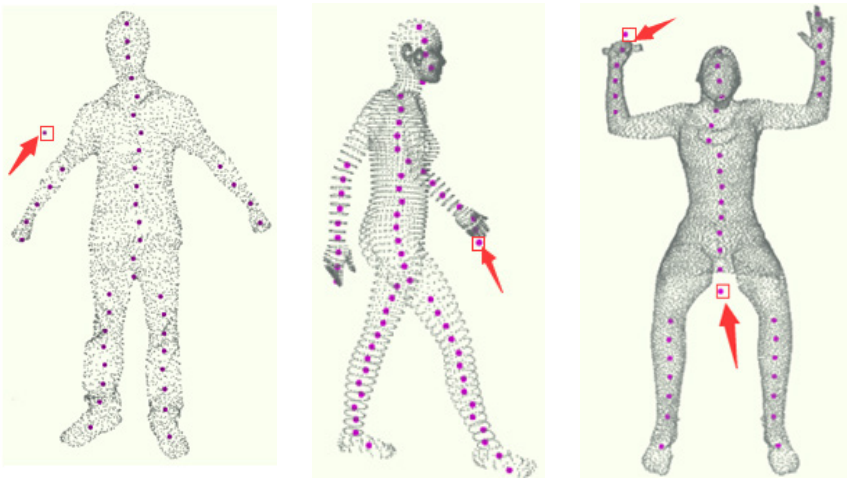

Fig. 8. Skeleton points of different human body gestures

4.3 Initial Skeleton Line Extraction

Skeleton Point Regularization. In order to remove those points outside the model from skeleton point set, it is necessary to judge whether these points are located outside or not. As shown in Fig. 9(a), the point located outside the projection region and the point located inside the projection region in Fig. 9(b). Non-Zero Winding Number Rule is adopted to remove those points outside the model. For a given curve C and a given point p: construct a ray (a straight line) heading out from p in any direction towards infinity. Find all the intersections of C with this ray. Score up the winding number as follows: for every clockwise intersection (the curve passing through the ray from left to right, as viewed from P) subtract 1; add 1 to every counter-clockwise intersection (curve passing from right to left, as viewed from P. If the total winding number is zero, P is outside C; otherwise, it is inside. Those point outside $\boldsymbol{C}$ could be removed as shown in Fig. 10.

(a) Outside the model (b) Inside the model

Fig. 9. Position of skeleton point

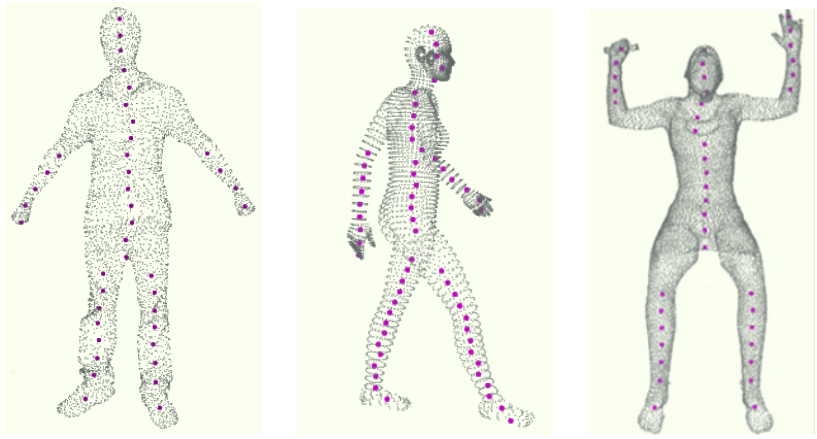

Fig. 10. Removing skeleton points outside the model

Skeleton Point Connection. The skeleton lines are acquired by two steps:

(1) connection of skeleton points belongs to one region;

(2) connection of skeleton points for different regions.

The skeleton points of each model part (such as the left arm, left leg etc.) have the same label, then the skeleton points in adjacent layer that belong to the same part is connected, and the initial skeleton line is obtained, as shown in Fig. 11.

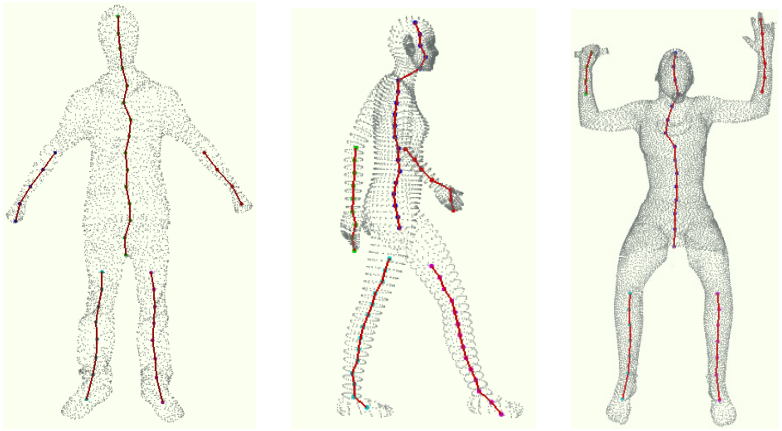

Fig. 11. Connection of the same part of human skeleton points

For different parts of body model, the connection of skeleton point is achieved according to the labels of skeleton points. Those points labeled as " M " are in main part of model, and the points labeled as " N " are in the branches of model. Connect those points labeled as " M " to those points labeled as " N " , then initial skeleton is generated.

Definition 1 Connection points. The connection point between the branch and the main body is joined, or the backbone of the main body and the branch, e.g., point q_1 and p_2 in Fig. 12.

Definition 2 Highest points. Point with maximum y coordinate in skeleton point set, e.g., point q_1 and p_1 in Fig. 12.

Definition 3 Lowest points. Points with minimum y coordinate in skeleton point set, e.g., point q_2 and p_3 in Fig. 12.

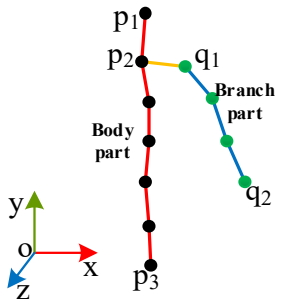

Fig. 12. Connection point, the highest and lowest point

Select a connection point from the branch and main parts respectively. The connection point for the branch parts is usually the highest or lowest point in this part. The highest point p_1 and the lowest point p_2 in skeleton set SKM of body part are obtained, and the highest point q_1 and the lowest point q_2 in skeleton set SKN of branch part are computed. Compare the y coordinate $y_{p_1}, y_{q_1}, y_{q_2}$, if $y_{q_1} \geq y_{p_1}$, then point q_2 is marked as the connection point; otherwise, the point q1is marked as the connection point.

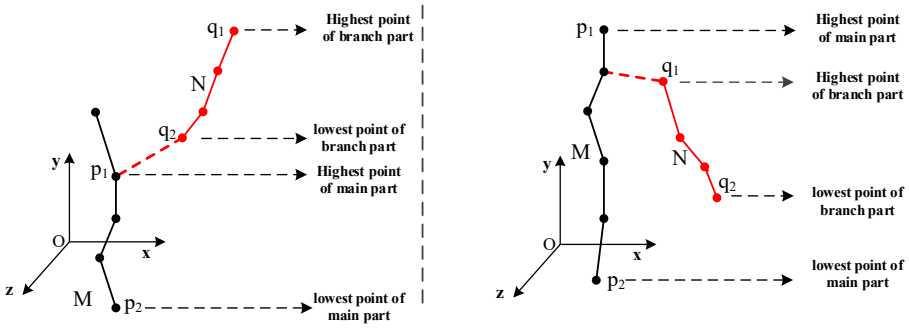

Fig. 13. Connection point in branch part

The connection point for the main part is determined according to the principle in Fig. 13. The point q is supposed to be the connection point in branch part, and q' is the skeleton point which belongs to the same branch as q and also closest to q, the point d is the search distance, p_i and p_j are two skeleton points that have the same distance to point q, α is the angle between p_iq and pq, θ is the angle between p_jq and pq. Starting from point q, search its nearest point p_i within d. If $\alpha \leq \theta$, then select p_i as the connection point of body part, otherwise select p_i. Here, the angle αand θ is calculated as the follows:

$$\alpha = \arccos\left(\frac{(x_1 - x_i)(x_1 - a) + (y_1 - y_i)(y_1 - b) + (z_1 - z_i)(z_1 - c)}{\left|\overrightarrow{qp_i}\right|\left|\overrightarrow{qp}\right|}\right). \tag{3}$$

$$\theta = \arccos\left(\frac{(x_1 - x_j)(x_1 - a) + (y_1 - y_j)(y_1 - b) + (z_1 - z_j)(z_1 - c)}{\left|\overrightarrow{qp_j}\right|\left|\overrightarrow{qp}\right|}\right). \tag{4}$$

The coordinates of the points q, q' are $q(x_1, y_1, z_1)$, $q'(x_2, y_2, z_2)$, and the coordinates of the points p_i, p_j are $p_i(x_i, y_i, z_i)$, $p_j(x_j, y_j, z_j)$. $d + k\xi$ is the searching range, where d stands for the search distance, k stands for

the number of searches and ξ stands for the step size in search. The initial skeleton lines are illustrated in Fig. 14. Initial skeleton lines for different human models are shown in Fig. 15.

$$a = \sqrt{\frac{(d+\kappa\xi)^2}{(x_2-x_1)^2+(y_2-y_1)^2+(z_2-z_1)^2}}(x_2-x_1)+x_1. \tag{5}$$

$$b = \sqrt{\frac{(d+\kappa\xi)^2}{(x_2-x_1)^2+(y_2-y_1)^2+(z_2-z_1)^2}}(y_2-y_1)+y_1. \tag{6}$$

$$c = \sqrt{\frac{(d+\kappa\xi)^2}{(x_2-x_1)^2+(y_2-y_1)^2+(z_2-z_1)^2}}(z_2-z_1)+z_1. \tag{7}$$

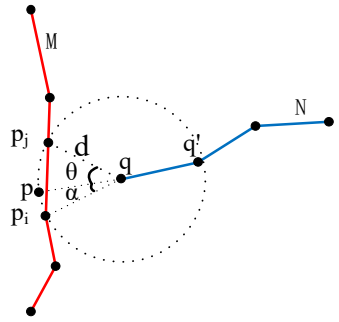

Fig. 14. Connection of skeleton lines between the main part and the branch part

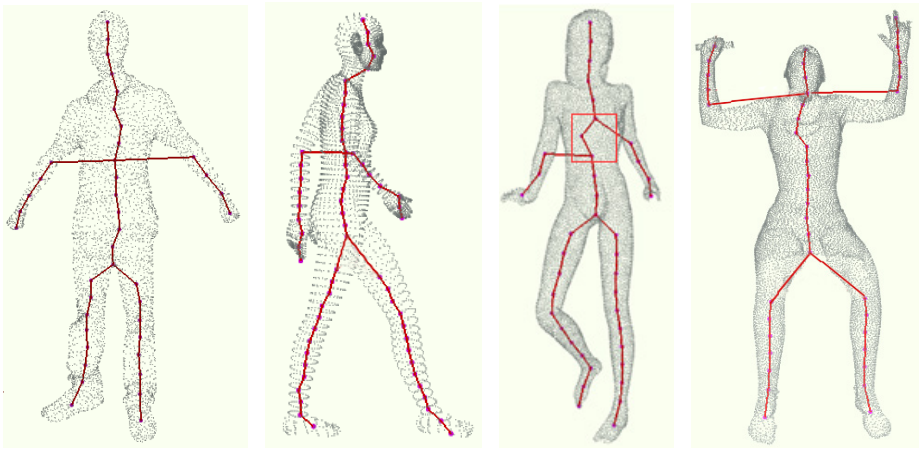

Fig. 15. Initial skeleton lines for different human models

4.4 Optimized Skeleton Line

The initial skeleton for body model has obtained, however, it may deviate from the center of body model due to complicated body action. Meanwhile, it also produces some bifurcation points and internal error branch. Therefore, the initial skeleton must be optimized two-step processing which contains rough processing and refined processing. The rough processing includes removing bifurcation point and internal branch noise, and makes

the model skeleton line centralization; and the refined processing is to discretize the skeleton by using interpolation points.

Bifurcation Point Processing. The existence of multiple bifurcation points (as shown in Fig. 16(a)) greatly affects the central and smoothness of skeleton line.

The wrong bifurcation points are found by calculating the number of those points with a degree of three. If the number of those points is 1, then there is no presence of bifurcation point. If the number of those points is greater than 1, then there is exists bifurcation points. Taking the point with the largest y coordinate as the reference point, the remaining wrong bifurcation point is replaced by the reference point, as shown in Fig. 16(b). The point p' in Fig. 16(b) is the result after removing the wrong bifurcation point p.

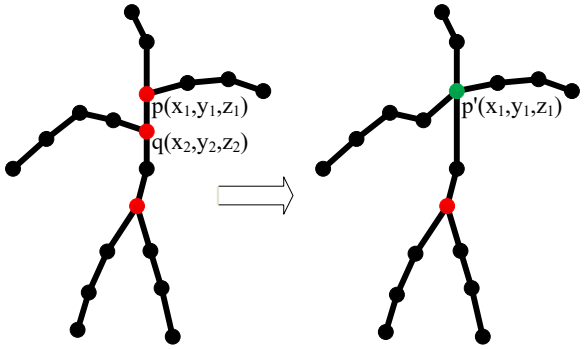

(a) Wrong bifurcation point (b) Result after optimization

Fig. 16. Skeleton lines optimization by removing the bifurcation point

Skeleton Centralization. Skeleton centralization is to move the skeleton line of the model into the center of body model. As in Fig. 17, the skeleton line in the armpit, hips and shoulders has appeared to be outside the skeleton model. To solve this problem, an interpolation-based method is proposed as illustrated in Fig. 18. The algorithm is illustrated in Table 2. After bifurcation line is processed, the result is shown in Fig. 19.

Table 2. Pseudo-code of skeleton centralization algorithm

	Algorithm. Skeleton centralization
	Input: Skeleton line
	Output: Optimized skeleton line
1	**For** each skeleton line
2	Calculate the skeleton point degree D
3	take those points with D = 4 or D = 3 as bifurcation point
4	find those skeleton lines that require optimization and the total number N
5	**End for**
6	**For** skeleton line to be optimized
7	Insert m interpolation point, e.g. $q_0 \sim q_{m-1}$
8	**For** each interpolation point
9	Search the neighboring point set V
10	Obtain the slice projection according to the interpolation point q_i and generate a banded set of points C
11	Compute the center o_i of C
12	move q_i to o_i
13	**End for**
14	connect $q_0 \sim q_{m-1}$
15	connect the connection point in branch part and q_0
16	connect the connection point in main part and q_{m-1}
17	**End for**

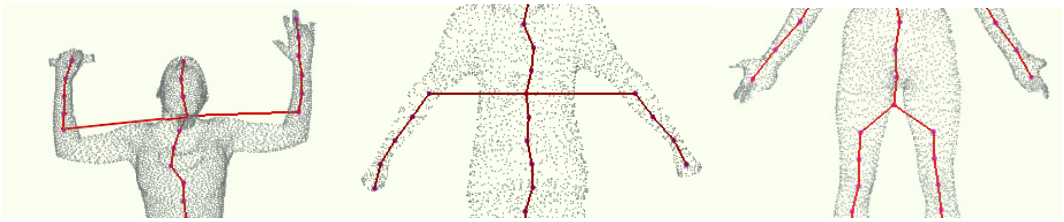

(a) Bifurcation line in shoulder (b) Bifurcation line in Armpit (c) Bifurcation line in Crotch

Fig. 17. Branching skeleton lines that need to be moved inside the model

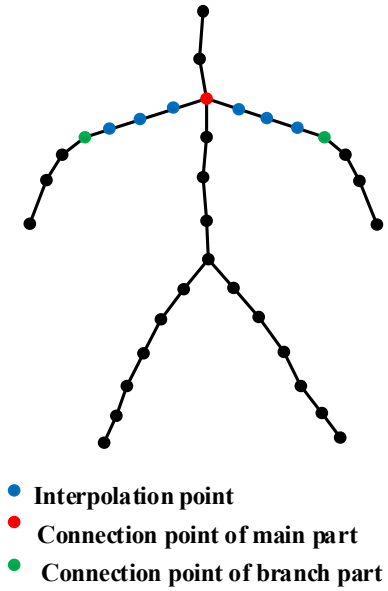

Fig. 18. The interpolation points

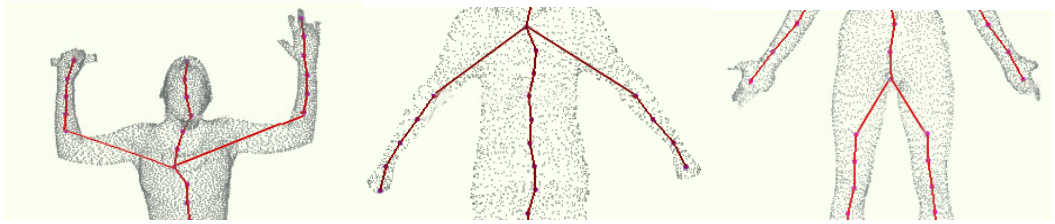

Fig. 19. Results of the skeleton lines after bifurcation line processing

5 Experimental Results

The scanned body model from Princeton shape Database is used to mainly evaluate the method in the paper, the proposed method is implemented on a standard workstation equipped with an Intel I7-12700 CPU (Octa core, 4.7 GHz) and NVDA RTX3060-6G graphics card, and programmed with VC++ and OpenGL for displaying and rendering.

5.1 Skeleton Extraction Result

In Fig. 20, the whole process of skeleton extraction method is illustrated, which is mainly executed in several steps: slicing, center point, skeleton connection, initial skeleton and optimized skeleton.

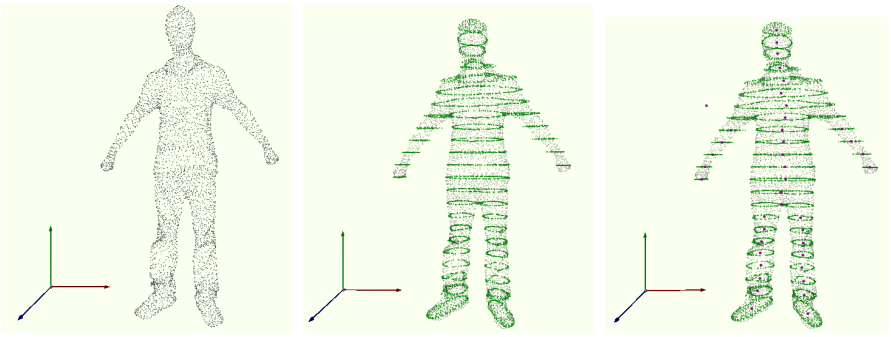

(a) Raw data (b) Slice projection (c) Center point

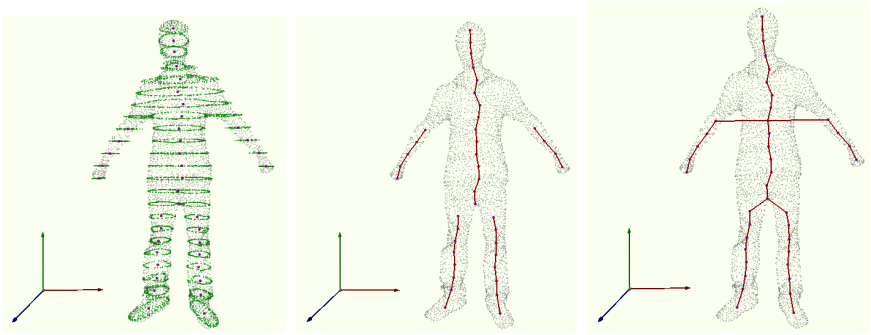

(d) Removing points outside (e) Main skeleton connection (f) Branch skeleton connection

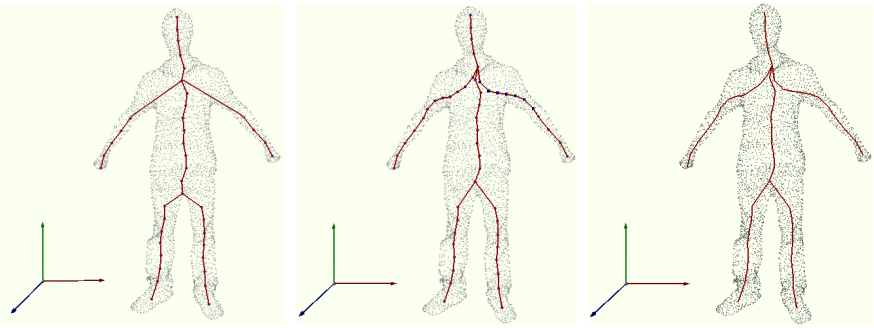

(g) Initial skeleton (h) Optimized skeleton (i) Final curve skeleton

Fig. 20. Skeleton extraction of the same model

5.2 Curve Skeleton for Body Model with Various Pose

The skeleton extraction method in the paper can deal with the human body model under different postures, the experimental parameters are shown in Table 3. Fig. 21 displays the skeleton line of the human model under different postures. The skeleton is shown from different views. Fig. 22 displays the skeleton for different human body model. Experiments show that the algorithm for extracting pose from the basic skeleton of the human body model has good adaptability and can automatically determine the optimized skeleton, the final model has better axial skeleton curve and smoothness.

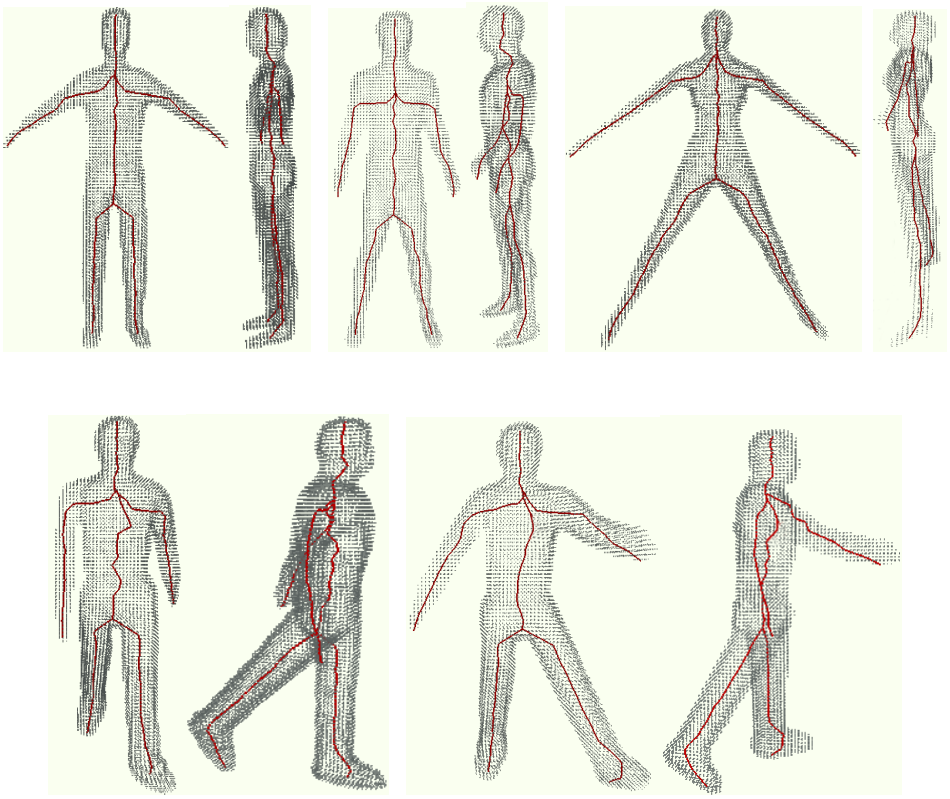

Fig. 21. Curve skeleton for same body model under different gestures

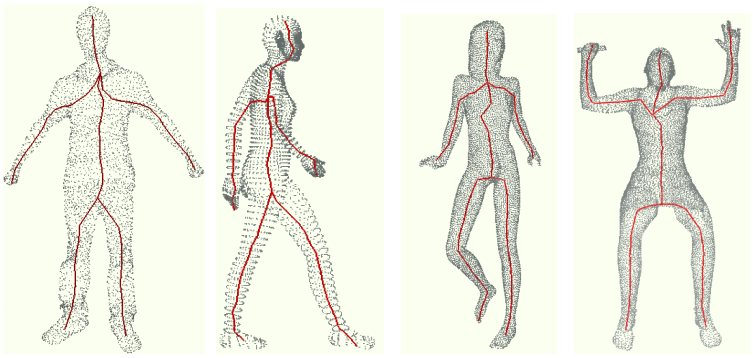

(a) Body1 model (b) Body2 model (c) Body4 model (d) Body5 model

Fig. 22. Curve skeleton for different body model

Table 3. The model and the experimental parameters

Model	Vertex number	Third	Mesh size(m)	Interpolation point number
Human model 1	7835	45	0.015	9
Body1	7521	23	0.03	7
Body2	9641	35	0.023	5
Body4	15015	22	0.015	5
Body5	20910	25	0.03	9

5.3 Performance Analysis

It can evaluate the algorithm in the paper on those data with missed parts, as shown in Fig. 23. The result demonstrates that it has good robustness to the original point cloud with missed parts, as shown in Fig. 24. The skeleton could keep good accuracy and centrality and adaptable to various model.

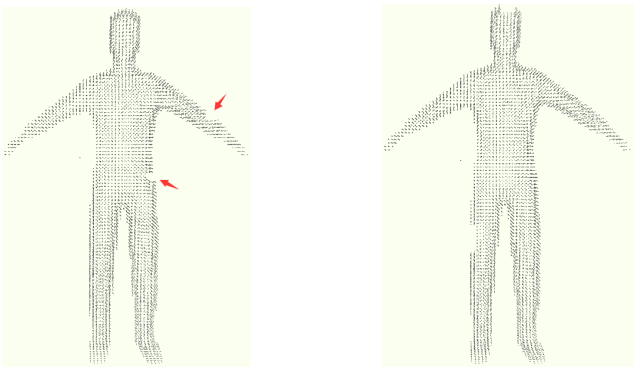

(a) Human5 model with small holes (b) Human6 model with large holes

Fig. 23. Model with holes

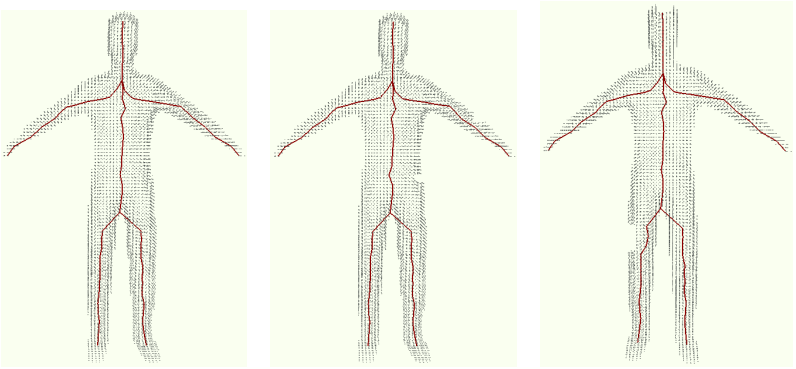

Fig. 24. Results of skeleton on model with holes

5.4 Comparison Results Analysis

The algorithm in the paper is proved to be more robust and adaptable than the traditional algorithm in [18] and [23], then it is also more efficient. The results are shown in Fig. 25 and Fig. 26.

Fig. 25 is the result of comparison with the literature [23]. In algorithm of [23], when the skeleton of the human body model is obtained, the skeleton at the joints is outside the model, which leads to the poor accuracy of the final skeleton extraction effect. In this case, our method does not have this problem, therefore, the final skeleton extraction accuracy of human body model is better than that in [23]. In addition, the skeleton of the human body model in [23] is not very good at the joint of the shoulder, but our algorithm is optimized for the skeleton line of the shoulder position. In contrast, the axiality of the model skeleton has been improved.

The skeleton of the human body model obtained in [18] is relatively poor in the central axis of the skeleton line on the shoulder, and multiple bifurcation points have occurred. In our method, the partial fork points in the model are specifically integrated, and multiple bifurcation points are avoided. Therefore, the axial and smoothness of the final skeleton line of the model is relatively good. Fig. 26 is the comparison results between our algorithm and literature [18].

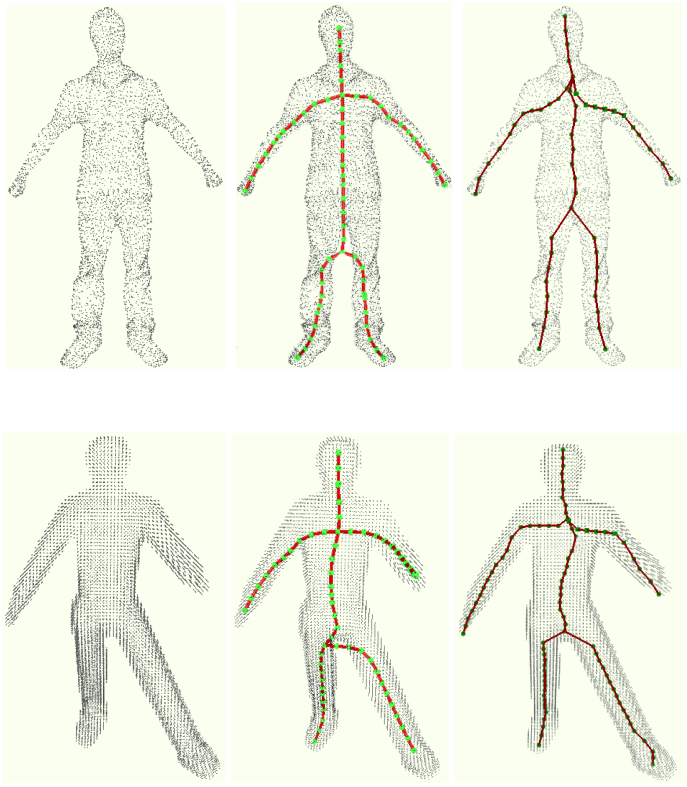

(a) Raw data (b) Reference [23] (c) Our algorithm

Fig. 25. Comparison results between our algorithm and reference [23]

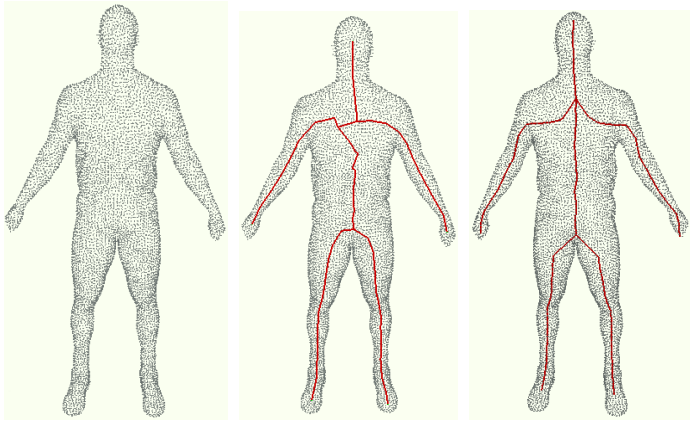

(a) Raw data (b) Reference [18] (c) Our algorithm

Fig. 26. Comparison results between our algorithm and reference [18]

6 Conclusion

In the paper, the novel algorithm for extracting curve skeleton from unorganized, incomplete and unoriented 3D point cloud body model is proposed. The algorithm firstly normalizes the body model according to the main trend of original point cloud data, then a horizontal slice-based method is proposed to extract a series of center points. The two-step skeleton line extraction principle which contains initial skeleton and optimized skeleton is adopted

to obtain more robust curve skeleton. Experimental results show that our method is capable of maintaining good robustness and efficiency for the skeleton extracted from incomplete point cloud data. Our method exhibits the advantages of the slicing guided skeleton extraction methods.

References

[1] X.-C. Li, WITHDRAWN: Human Body model Bone Extraction Algorithm based on Space Segmentation and Computer Image, Microprocessors and Microsystems 12(5)(2021) 39-44.

[2] X.-T. Li, T.W. Woon, T.S. Tan, Z.-Y. Huang, Decomposing Polygon Meshes for Interactive Applications, in: Proc. of the 2001 Symposium on Interactive 3D graphics, 2001.

[3] T.K. Dey, J. Sun, Defining and Computing Curve-skeletons with Medial Geodesic Function, in: Proc. of Eurographics Symposium on Geometry Processing, 2006.

[4] H. Martin, R. Fernandez, Y. Khoo, Large Angle based Skeleton Extraction for 3D Animation. <https://arxiv.org/abs/1608.05045>, 2016 (accessed 17.08.2016).

[5] F.-C. Wu, W.-C. Ma, R.-H. Liang, B.-Y. Chen, M. Ouhyoung, Domain connected graph: The Skeleton of a Closed 3D Shape for Animation, The Visual Computer 22(2)(2006) 117-135.

[6] Y.-L. Tu, W.-Y. Lin, Y.-C. Lin, Toward automatic plant phenotyping: starting from leaf counting, Multimedia Tools and Applications 81(9)(2022) 11865-11879.

[7] Z.-M. Chen, J.-J. Pan, X.-S. Yang, H. Qin, Hybrid Features for Skeleton-based Action Recognition based on Network Fusion, Computer Animation and Virtual Worlds 31(4-5)(2020) e1952.

[8] Y. Shu, X. Yang, A Fast Skeleton Extraction Algorithm for 3D Cartoon Character, Journal of Donghua University (Natural science) 44(4)(2018) 503-507.

[9] K.-L. He, Y. X, A.-H. Mao, G.-Q. Li, Rapid 3D human body modeling based on Kinect technology, Computer Aided Drafting, Design and Manufacturing 23(1)(2022) 11-17.

[10] Y. Zhang, F. Tan, S.-F. Wang, B.-C. Yin, 3D Human Body Skeleton Extraction from Consecutive Surfaces using a Spatial–temporal Consistency Model, The Visual Computer 37(5)(2021) 1045-1059.

[11] C. Yang, B. Indurkhya, J. See, M. Grzegorzek, Towards Automatic Skeleton Extraction with Skeleton Grafting, IEEE Transactions on Visualization and Computer Graphics 27(12)(2021) 4520-4532.

[12] H.-L. Hu, Z. Li, X.-G. Jin, Z.-G. Deng, M. Chen, Y. Shen, Curve Skeleton Extraction From 3D Point Clouds Through Hybrid Feature Point Shifting and Clustering, Computer Graphics Forum 39(6)(2020) 111-132.

[13] A. Tagliasacchi, H. Zhang, D. Cohen-Or, Curve Skeleton Extraction from Incomplete Point Cloud, ACM Transactions on Graphics 28(3)(2009) 1-9.

[14] N.D. Cornea, D. Silver, P. Min, Curve-skeleton Properties, Applications, and Algorithms, IEEE Transactions on Visualization and Computer Graphics 13(3)(2007)530-548.

[15] A.C. Jalba, A. Sobiecki, A.C. Telea, An Unified Multiscale Framework for Planar, Surface, and Curve Skeletonization, IEEE transactions on pattern analysis and machine intelligence 38(1)(2016) 30-45.

[16] W. Jiang, K. Xu, Z.-Q. Cheng, R.R. Martin, D. Gang, Curve skeleton extraction by coupled graph contraction and surface clustering, Graphical Models 75(3)(2013) 137-148.

[17] A.P. Mangan, R.T. Whitaker, Partitioning 3D Surface Meshes using Watershed Segmentation, IEEE Transactions on Visualization and Computer Graphics 5(4)(1999) 308-321.

[18] J.-J. Cao, A. Tagliasacchi, M. Olson, H. Zhang, Z.-X. Su, Point Cloud Skeletons via Laplacian Based Contraction, in: Proc. SMI 2010, Shape Modeling International Conference, 2010.

[19] W. Deng, K. Luo, Q.-K. Shi, Y. Yang, N. Ning, Automatic Segmentation and Diagnosis Based on Multi-Scale Two-Stage Region Growing and Skeleton Extraction for Vessel Stenosis in Coronary Angiography, Journal of Medical Imaging and Health Informatics 10(2)(2020) 446-451.

[20] K. Arhid, F.R. Zakani, M. Bouksim, M. Aboulfatah, T. Gadi, An Efficient Hierarchical 3D Mesh Segmentation Using Negative Curvature and Dihedral Angle, International Journal of Intelligent Engineering and Systems 10(5)(2017) 143-152.

[21] N. Gelfand, L.J. Guibas, Shape Segmentation using Local Slippage Analysis, in: Proc. ACM SIGGRAPH symposium on geometry processing, 2004.

[22] C.-X. Liu, C. Tang, M. Xu, F.-G. Hao, Z.-K. Lei, Skeleton Extraction and Inpainting from poor, broken ESPI Fringe with M-net Convolutional Neural network, Applied Optics 59(17)(2020) 5300-5308.

[23] H. Huang, S.-H. Wu, D. Cohen-Or, M.-L. Gong, H. Zhang, G.-Q. Li, B.-Q. Chen, L_1-medial skeleton of point cloud, Acm Transactions on Graphics 32(4)(2013) 65.

[24] C.M. Ma, M. Sonka, A Fully Parallel 3D Thinning Algorithm and Its Applications, Computer Vision & Image Understanding 64(3)(1996) 420-433.

[25] C.-M. Ma, S.-Y. Wan, A Medial-surface Oriented 3-D two-Subfield Thinning Algorithm, Pattern Recognition Letters 22(13)(2001) 1439-1446.

[26] W.-J. Che, X.-N. Yang, G.-Z. Wang, A Dynamic Approach to Skeletonization, Journal of software 14(4)(2003) 818-823.

[27] C. Lohou, G. Bertrand, Two symmetrical thinning algorithms for 3D binary images, based on P-simple points, Pattern

Recognition 40(8)(2007) 2301-2314.
[28] T. Wang, I. Cheng, Generation of Unit-Width Curve Skeletons Based on Valence Driven Spatial Median (VDSM), in: Proc. International Symposium on Advances in Visual Computing, 2008.
[29] O. Sorkine, D. Cohen-Or, Least-Squares Meshes, in: Proc. of Shape Modeling, 2004.
[30] O.K.C. Au, C.L. Tai, H.K. Chu, D. Cohen-Or, T.Y. Lee, Skeleton Extraction by Mesh Contraction, ACM Transactions on Graphics 27(3)(2008) 1-10.
[31] A. Nealen, T. Igarashi, O. Sorkine, M. Alexa, Laplacian Mesh Optimization, in: Proc. International Conference on Computer Graphics and Interactive Techniques in Australasia and Southeast Asia, 2006.
[32] P. Hou, Q.-G. Tian, B.-Z. Ge, Research on method of extracting skeletal curves of 3D human scanning data based on optimizing DRG, Computer Engineering and Applications 50(18)(2014) 182-187.
[33] A. Tagliasacchi, I. Alhashim, M. Olson, H. Zhang, Mean Curvature Skeletons, Computer Graphics Forum 31(5)(2012) 1735-1744.
[34] S.-L. Lu, G. Li, J. Wang, A Novel Method for Extracting Skeleton of Fruit Tree from 3D Point Clouds, International Journal of Modeling, Simulation, and Scientific Computing 11(6)(2020) 2050051.
[35] Y. Lipman, D. Cohen-Or, D. Levin, H. Tal-Ezer, Parameterization-free Projection for Geometry Reconstruction, ACM Transactions on Graphics 26(3)(2007) 22-es.
[36] S. Katz, A. Tal, Hierarchical Mesh Decomposition Using Fuzzy Clustering and Cuts, ACM Transactions on Graphics (TOG) 22(3)(2003) 954-961.
[37] M. Livesu, F. Guggeri, R. Scateni, Reconstructing the Curve-Skeletons of 3D Shapes Using the Visual Hull, IEEE transactions on visualization and computer graphics 18(11)(2012) 1891-1901.
[38] A. Zimovnov, L. Mestetskiy, Curve-skeleton Extraction from Visual Hull, in: Proc. of the 10th International Conference on Computer Vision Theory and Applications (VISAPP), 2015.
[39] M.S. Hassouna, A.A. Farag, Robust Centerline Extraction Framework using Level Sets, in: Proc. on Computer Vision and Pattern Recognition, 2005.
[40] Y. Zhou, A.W. Toga, Efficient Skeletonization of Volumetric Objects, IEEE Transactions on Visualization and Computer Graphics 5(3)(1999) 196-209.
[41] L. Wade, R.E. Parent, Automated Generation of Control Skeletons for Use in Animation, The Visual Computer 18(2) (2002) 97-110.
[42] I. Bitter, A.E. Kaufman, M. Sato, Penalized-distance Volumetric Skeleton Algorithm, IEEE Transactions on Visualization and Computer Graphics 7(3)(2001) 195-206.
[43] N.D. Cornea, D. Silver, X. Yuan, R. Balasubramanian, Computing Hierarchical Curve-skeletons of 3D Objects, The Visual Computer 21(11)(2005) 945-955.
[44] W.-C. Ma, F.-C. Wu, M. Ouhyoung, Skeleton Extraction of 3D Objects with Radial Basis Functions, in: Proc. of the Shape Modeling International, 2003.